Variation in Mineral Properties in Normal and Mutant Bones and Teeth

Adele L. Boskey[a]   Marian F. Young[b]   Tina Kilts[b]   Kostas Verdelis[a]

[a]Mineralized Tissue Research Laboratory, Musculoskeletal Integrity Program, Hospital for Special Surgery, New York, N.Y., and [b]National Institute of Dental and Craniofacial Research, National Institutes of Health, Bethesda, Md., USA

Abstract

Hydroxyapatite mineral is deposited in an organized fashion in the matrices of bones and teeth. The amount of mineral present, the composition of the mineral, and the size of the mineral crystals varies with both tissue and animal age, diet, health status, and the tissue being examined. Here, we review methods for measuring these differences in mineral properties and provide some illustrations from bones and teeth of animals in which the small leucine-rich proteoglycans (biglycan and decorin) were ablated. Differences in mineral properties between biglycan-deficient bones and teeth are related to the functions of this small proteoglycan in these tissues.

Copyright © 2005 S. Karger AG, Basel

Introduction

The mineral in physiologically calcified tissues is an analogue of the geologic mineral, hydroxyapatite [HA; $Ca_{10}(PO_4)_6(OH)_2$]. Bone, dentin, and cementum crystals deposit upon a collagen template in an oriented fashion [Robey, 1996] and tend to be relatively small, having a large portion of their unit cells on their surface. This small size leads the crystals to have many adsorbed ions and imperfections [Posner and Beebe, 1975], causing the Ca/P ratio to vary significantly from the stoichiometric 10:6 ratio [Peru and Daculsi, 1994]. The crystals in enamel, not formed on a collagen matrix, are significantly larger and have fewer impurities than those in bone, dentin, and cementum [Bonar et al., 1991].

There are a number of physical and chemical techniques that have been used to characterize the mineral in these tissues. The nature of the phase present and the av-

Abbreviations used in this paper	
BGN	biglycan
DCN	decorin
DMP-1	dentin matrix protein 1
FTIR	Fourier transform infrared spectroscopy
FTIRI	Fourier transform infrared imaging spectroscopy
HA	hydroxyapatite
KO	knockout
NIDCR	National Institute of Dental and Craniofacial Research
PCR	polymerase chain reaction
PMMA	polymethylmethacrylate
SLRP	small leucine-rich proteoglycan
WT	wildtype

Adele L. Boskey, PhD
Mineralized Tissue Research Laboratory
Musculoskeletal Integrity Program, Hospital for Special Surgery
535 E 70th St., New York, NY 10021 (USA)
Tel. +1 212 606 1453, Fax +1 212 472 5331, E-Mail boskeya@hss.edu

erage size/perfection of the crystals is usually determined by wide-angle X-ray or electron diffraction [Boskey, 2001]. Such analyses require either the presence of single crystals (not feasible with these tissues) or homogenization of the tissue prior to analysis. The sizes, shapes, and orientation of the crystals with respect to the underlying matrix can be determined by electron microscopic techniques including scanning, transmission, and atomic force microscopy [Landis et al., 1984; Kirkham et al., 1998; Tong et al., 2003], and the ionic composition can be determined by chemical analyses or electron microprobe analyses [Akesson et al., 1994]. The distribution of the mineral within the tissue can be determined by backscatter electron imaging [Roschger et al., 1995], microcomputed tomography (CT) [Genant et al., 2000], or radiographic techniques using appropriate standards. Unique information about the spatial distribution of both mineral and matrix can be obtained by vibrational spectroscopic techniques such as infrared and Raman spectroscopy and spectroscopic imaging [Boskey and Mendelsohn, 2005].

The nature, properties, and distribution of these properties of the mineral in calcified tissues affect the ability of the tissue to be remodeled and, more significantly, the mechanical strength of the tissue [Boskey, 2003]. The nature of the matrix upon which the crystals are deposited, along with physicochemical factors, determines these properties. Analyses of changes in mineral (and matrix properties) in healthy and diseased tissues as well as in the mineralized tissues of genetically modified animals provide insights into the functions of specific matrix components on the properties of the tissues. For example, mice with the gene for osteocalcin ablated, while initially reported to have thickened bones [Ducy et al., 1996] suggesting osteocalcin was regulating bone formation, were later shown to have smaller crystals that did not remodel based on infrared microspectroscopy [Boskey et al., 1998], indicating the importance of osteocalcin in bone remodeling. Similarly, analysis of the bones of the osteopontin knockout (KO) mouse demonstrated the importance of osteopontin for the regulation of crystal size – crystals were larger and more perfect than in the wildtype (WT) controls – as well as its role in osteoclast recruitment [Boskey et al., 2002]. Mice lacking dentin matrix protein 1 (DMP-1), a protein produced abundantly by hypertrophic chondrocytes and osteoblasts [Feng et al., 2003], had decreased bone density and osteomalacia with decreased mineral content and increased crystal size [Ling et al., 2005], showing that DMP-1 (or some fragment thereof) was acting as a mineral nucleator. In this paper,

we illustrate the use of vibrational spectroscopy and micro-CT for the study of teeth as well as bones of mice lacking one of the small leucine-rich proteoglycans (SLRPs), decorin (DCN) or biglycan (BGN). The properties of the bones of the BGN-KO mice have been described previously [Xu et al., 1998], but in less detail than in this review. The bones of BGN-KO mice, while normal at birth, appeared osteopenic with advancing age, developing thin widely spaced trabeculae, a decreased mineral content, and increased crystal size at bone-forming sites.

The SLRPs belong to the leucine-rich repeat superfamily of proteins [Hocking et al., 1998] which, as reviewed elsewhere [Ameye and Young, 2002], is characterized by domains of disulfide bond-forming cysteine-rich clusters, flanking the central leucine-rich repeats. The SLRPs are small in relation to the large proteoglycans such as aggrecan and versican [Iozzo, 1998]. DCN, BGN and some other SLRPs bind to collagen and transforming growth factor-β, and through these interactions, are not only involved in the regulation of collagen fibril size but also appear to be involved in cell proliferation and differentiation [Ameye and Young, 2002]. BGN deficiency tends to result in increased collagen fibril diameter in bone [Corsi et al., 2002] and in decreased diameter during dentin development [Goldberg et al., 2003].

Part of the effect of BGN deficiency on bone development is related to changes in cell proliferation. In vitro, the number of bone marrow stromal cells decreases more rapidly in BGN-KO than in WT mice [Chen et al., 2002]. These cells, which are osteoblast precursors, also produce less type I collagen in culture, suggesting that the matrix in the BGN-KO animals may be abnormal. BGN in solution is a HA nucleator [Boskey et al., 1997] which, in combination with the abnormal matrix that forms in the absence of BGN, may explain why there is a lower mineral content in the bones of the BGN-KO mice. In the jaw, a day after birth, the BGN-KO first molar shows altered dentin mineralization [Goldberg et al., 2003], and structural defects are also observed in forming enamel, with increasing thickness.

DCN-KO mice [Danielson, 1997] show abnormal collagen fibrillogenesis in skin and tendon. In contrast to the BGN-KO mice, the DCN-deficient animals were not reported to show alterations in bone mass, or any other major phenotypic changes in bone at the histological or macroscopic level [Corsi et al., 2002]. In this review, we illustrate how micro-CT and Fourier transform infrared imaging (FTIR) microspectroscopy provide new insight into the mineral and matrix properties of the BGN- and DCN-deficient teeth and the BGN-deficient bones.

Materials and Methods

Animals

WT, BGN-KO, and DCN-KO mice were generated at the National Institute of Dental and Craniofacial Research (NIDCR) under an institutionally approved protocol for the use of animals in research (NIDCR 98-058 and 03-280). The mice used in this experiment were generated by backcrossing the original BGN-KO and DCN-KO strain (129B6/C57 mixture), i.e. strains were maintained separately, for over ten generations. In some experiments, the 129 B6/C57 BGN-KO and DCN-KO mice were backcrossed with the C3H/HeNHsd strain to a purity greater than 95% (in this study, indicated as C3H strain). Approximately 2 mm of the tip of the tail was removed from animals just after weaning (approximately 21 days) and DNA extracted using the commercial purification kit Highpure (Invitrogen). Purified DNA (10 μl) was used for a polymerase chain reaction (PCR)-based genotype assay consisting of $1\times$ PCR buffer with $MgCl_2$ (Invitrogen), 0.2 mM dNTP, and 2 ng of the following two primers: BGN exon 2, 5 prime end (forward) 5′caggaacattgaccatg3′, and BGN exon 2, 3 prime end (reverse) 5′gaaaggacacatggcactgaag3′. These primers detected the WT allele yielding a PCR band of 212 bp. A PGK1 primer (backward) 5′tggatgtggaatgtgtgcgagg3′ was used with the BGN exon 2, 5′ primer to detect the BGN-KO allele that was 310 bp. The overall genotype strategy to detect the DCN-KO allele was similar to that used to detect the BGN-KO alleles except that DCN exon 2, 5 prime end (forward) 5′ccttctggcacaagtctcttgg3′, and DCN exon 2, 3 prime end (backward) 5′tcgaagatgacactggcatcgg3′ primers were used to detect the WT DCN allele of 161 bp. The DCN-KO allele was detected as a 238-bp product when the DCN exon 2, 5 prime primer and PGK1 primer (see above) were used in combination. The PCR reactions were carried out by heating them at 95°C for 5 min prior to the addition of 0.5 μl AmpliTaq Gold Polymerase (Invitrogen). The PCR reaction was carried out with 35 cycles of a three-tiered program consisting of 95°C for 1 min, 57°C for 20 s, and 72°C for 30 s. The reaction was terminated by incubating the mixture at 72°C for 7 min. The resulting PCR products were separated by electrophoresis and visualized by staining with ethidium bromide. After analysis of each genotyping reaction, WT (+/0) and BGN-KO (–/0) males and WT (+/+) and BGN-KO (–/–) females, or WT (+/+) or DCN-KO (–/–) males or females were identified and housed separately until the time of tissue harvest. Mice of the desired age were euthanized by CO_2 inhalation and dissected using aseptic procedures. After decapitation, the skin was carefully removed from the head and the remaining experimental material placed in sterile gauze soaked in phosphate-buffered saline. The dissected tissue was immediately placed on dry ice and stored at –80°C until further analysis.

Tissue Samples

Mice for all the studies were provided by one of the authors from the collection at NIDCR. Mice for the teeth (jaw) studies were derived from the C3H background, and mice for the bone studies from the 129B6/C57 background. The jaws from BGN-deficient mice and their WT controls and from DCN-deficient mice and their WT controls used in the FTIR imaging (FTIRI) studies came from 3-month-old male mice. Extracted first and second molars from 6- to 7-month-old male and female BGN-deficient and WT animals were used in the micro-CT analysis. The mice for the BGN-deficient bone study (all males, 129B6/C57) were derived by gene targeting in embryonic stem cells [Xu et al., 1998], and the genotype was verified by PCR.

For FTIRI, the posterior parts of mouse hemi-jaws were dissected, cleaned of soft tissue, fixed in 90% ethanol, dehydrated through a series of solvents, and embedded in polymethylmethacrylate (PMMA). PMMA blocks were sectioned at 2–3 μm using a sliding microtome (Leica SM 2500, Leica, Germany), and sections were placed on BaF_2 windows for analysis.

Infrared Analyses of Teeth of WT and Mutant Animals

Semi-thin (2–3 μm) sections of the 3-month-old BGN- and DCN-deficient mouse molars and WT control molars were examined by FTIRI to acquire spectral images using the Perkin Elmer Spotlight Imaging system (Perkin Elmer Instruments, Shelton, Conn., USA). The spectral resolution was 8 cm^{-1} and the entire tooth section was scanned in each image, with 2–3 replicates per tooth. The spatial resolution was approximately 7 μm. Spectra were transferred to yield images corresponding to infrared band areas, peak height ratios and integrated area ratios by a combination of instrument software and ISYS chemical imaging software (version 2.1, Spectral Dimensions Inc., Olney, Md., USA) [Boskey and Mendelsohn, 2005]. Background spectra were collected under identical conditions from the same BaF_2 windows. After acquisition, spectra were truncated to allow analysis of the spectral data of interest, baseline was corrected, and the spectral contribution of the PMMA-embedding media was subtracted using ISYS software.

The spectroscopic parameters calculated were: mineral-to-matrix ratio, carbonate-to-matrix ratio, crystallinity, and collagen cross-link ratio. The mineral-to-matrix ratio – v1, v3 PO4 band (900–1,200 cm^{-1})/amide I band (1,590–1,720 cm^{-1}) integrated areas ratio – is linearly related to ash weight. Mineral crystallinity corresponds to the crystallite size and perfection as determined by X-ray diffraction and was calculated from the intensity ratios of subbands at 1,030 (stoichiometric apatite) and 1,020 cm^{-1} (non-stoichiometric apatite). The cross-link ratio is a parameter reflecting the maturity of the collagen, expressed as the absorbance ratio at two specific wave numbers (1,660 and 1,690 cm^{-1}). In the spectral images, pixels devoid of tissue (no mineral and/or matrix spectral signature) were set equal to zero and excluded from calculations. The spectroscopic results were expressed as histograms describing the pixel distribution of the parameters, mean values and standard deviations of the pixel distribution, and corresponding color-coded images were generated at the same time by ISYS.

Micro-CT

Mineral density of dentin and total volume of the crown of the BGN-deficient, DCN-deficient, and WT molars were calculated by quantitative micro-CT (Enhanced Vision Systems Model MS-8 in vitro micro-CT scanner, GE Healthcare, London, Ont., Canada). First and second molars from WT and KO animals were extracted from the mouse jaws using dental micro-spoon excavators, and their roots were cleaned of alveolar bone remains through careful use of a periodontal curette. Molars from 3 male and 4 female hemi-jaws were analyzed in both WT and KO groups (n_{total} = 28). The extracted molars were then positioned in a 70% alcohol-filled plastic container and fixed, while a calibration phantom was fixed in the same container. Two-dimensional projections of all the molars at the same time were collected by Evolver software (GE Healthcare) in three consecutive scans; the isotropic voxel size was 12 × 12 × 12 μm. The hardware of the Enhanced Visions System micro-

CT scanner employs filtering of the low-energy portion of the X-ray spectrum with aluminum, acrylic, and a saline bath to minimize beam hardening associated with polychromatic X-ray and to ensure uniformity of the beam at the detector array. To minimize noise, a large number of views (400), increased frame averaging, and increased shutter exposure time (3,000 ms) were utilized resulting in 4-hour scans. Each scan of the phantom containing air, saline and a bone reference material (1.18 g/cm^3) gave calibration in Hounsfield units to mineral density in grams per cubic centimeter. Scanner linearity was previously established by the manufacturer with a phantom containing nine densities of similar calibration material (Gammex RMI, Middleton, Wisc., USA). Reconstruction of projections into CT volume data was accomplished by Beam software (GE Healthcare) with a modified Parker algorithm [Tommasini et al., 2005]. A sub-volume was selected in Microview software (GE Healthcare) to segregate each molar for reconstruction.

The crowns were reoriented so that the cervical circumference lay, as much as possible, on the final x-plane, at which point all the mineralized structure that was above the x-plane was defined as the anatomical crown, and the part of the sample that was below the x-plane was defined as the root. The smallest parallelepiped sub-volumes into which the entire crown or roots could fit were positioned around each of these, respectively. Attenuation histograms of the volumes of interest were generated and Hounsfield units versus frequency values exported to Microsoft Excel for further processing. Individual thresholds were selected based on mineral density distribution for each molar, due to the fact that the transition between mineralized tissue and background soft tissue is very clear in our samples under the conditions used (fig. 3, histogram). An additional threshold was selected between dentin and enamel density distribution curves in crowns. Dentin mineral density for crowns and roots was computed based on density distribution between the two thresholds and the total volume crown, based on the total number of voxels with a density above the background-mineralized tissue threshold. Values for each of the three parameters (mineral dentin density in crown, in root, and crown volume) in every molar from all three scans were averaged, in order to reduce experimental error associated with factors such as X-ray scattering by very dense enamel, or operator bias (e.g., precise positioning of the crown cervix) in data processing.

Results

Infrared Microspectroscopy of BGN-KO and WT Bones

We have previously reported that there was increased crystallinity and a decreased mineral content in the bones of the male BGN-KO mice [Xu et al., 1998], although the data were not shown in that publication. We also reported that by 6 months of age, there were fewer trabeculae detectable in the KO than in the WT mice. Properties of the cortical bone, displayed as a function of location in the cortical bone, are summarized in figure 1a–c. In WT mice, as the animal ages, there is an initial increase in mineral content (fig. 1a) at all tissue sites, but at 6 months,
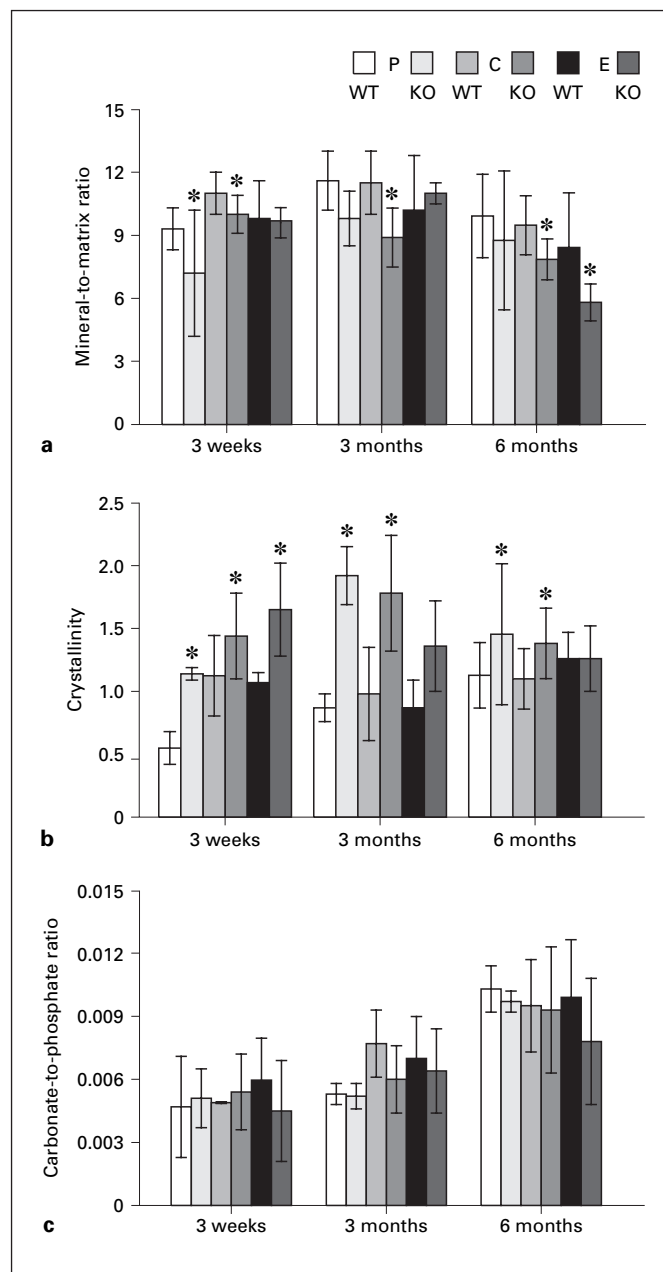

Fig. 1. FTIR microspectroscopic analysis of the bones of male BGN-KO and age- and sex-matched WT mice. Mean values from multiple (5–12) spectra obtained mid-shaft in each of three regions are shown. The mineral-to-matrix ratio (**a**) is decreased at all tissue sites except in the endosteum at all 3 ages, although statistical significance (* $p < 0.05$) was not found at 6 months in the periosteal region. Crystallinity (**b**) was significantly increased in KO in relation to WT mice in all but the endosteal regions at all time points. The carbonate-to-phosphate ratio (**c**) did not vary significantly between KO and WT mice at any time point, although values did increase significantly with time in each group, and the KO values tended to be decreased in older tissues at later time points. P = Bone adjacent to the periosteal surface; C = bone in the center of the cortex; E = bone adjacent to the endosteum.
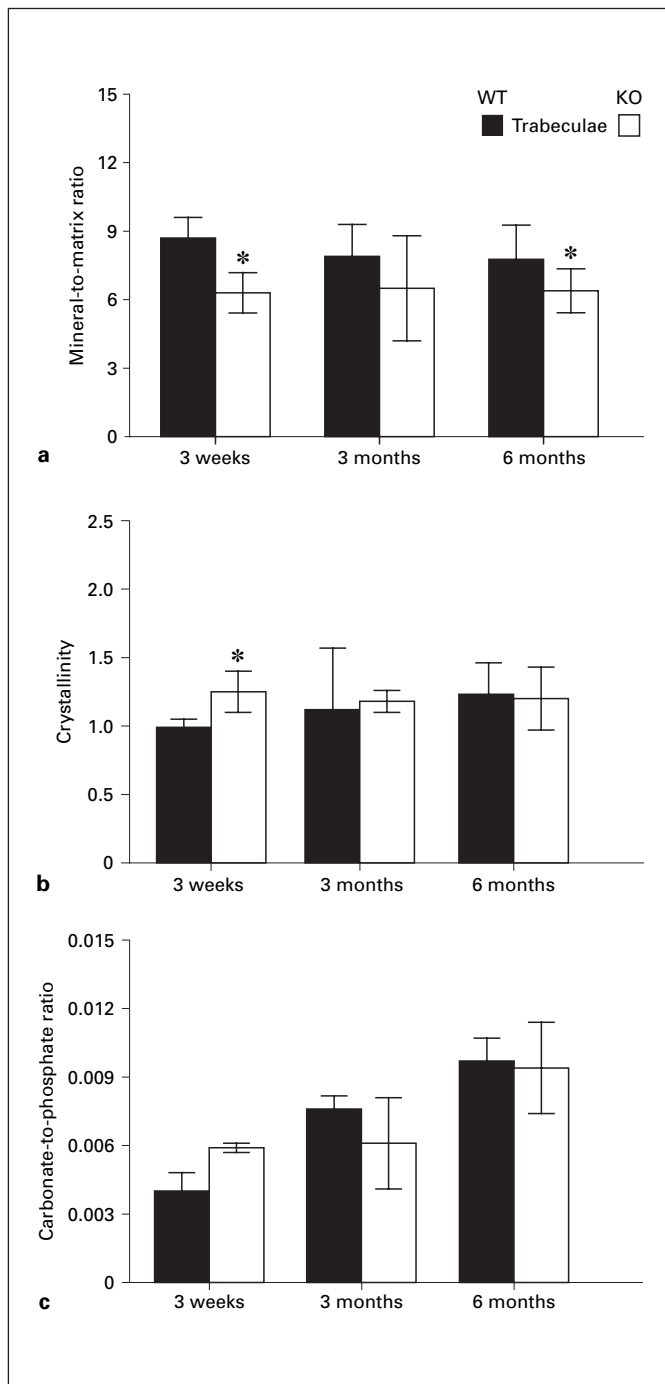
the mineral content decreased slightly. In contrast, in the KO mice, the mineral content at all sites other than the mineral adjacent to the endosteum was decreased in relation to age-matched controls. At 6 months, there was a significant decrease in the mineral content of the endosteum. The crystallinity, an indication of crystal size and perfection, increased with animal age at all tissue sites in the WT mice, and was significantly higher at all sites and ages in the KO mice (fig. 1b). In the endosteal region, crystallinity was comparable with WT mice at 6 months. The carbonate-to-phosphate ratio increased with animal and tissue age (where periosteal bone is younger than bone in the central cortex, and younger than the endosteal bone) in the WT mice, and was not significantly different in the KO mice when similar sites and animal ages were compared (fig. 1c).

Examining the same parameters in the trabecular bone, again, there is a decreased mineral content in the BGN-KO bone compared with the control (fig. 2a), but in contrast to the cortical bone, the mineral content remained constant as a function of age in both the WT and the KO trabeculae. Crystallinity was again increased in the BGN-KO mice (fig. 2b), but the difference between WT and KO mice was only significant in the youngest animals. The carbonate-to-phosphate ratio in the trabecular bone (fig. 2c) also tended ($p = 0.06$) to be higher in the youngest BGN-KO mice, but was equivalent at all other time points.

Micro-CT of BGN-KO Teeth

Micro-CT was used to measure the properties of the BGN-deficient animals in relation to age- and sex-matched controls at 3 months. The tooth crown as defined by the area of interest is shown in 3-dimensional rendering of a first WT molar (fig. 3a). Both crown and root mineral dentin densities were not significantly different between WT molars in male or female animals and their KO counterparts (data not shown). Although the interface between dentin and enamel voxels (fig. 3b, arrows) is not very steep, as it is likely that some enamel voxels have mineral density values which are very similar to high-mineral-density dentin voxels, distribution of mineral density in dentin was reproducible between scans. Figure 3c shows the measurement of the total crown volume (dentin and enamel) for male and female BGN-KO and WT control first molars (7 each, total specimens = 28). While there is essentially no difference between male WT and KO animals, crowns of first molars in female BGN-KO animals were significantly smaller (approximately 10%) than in their WT counterparts.
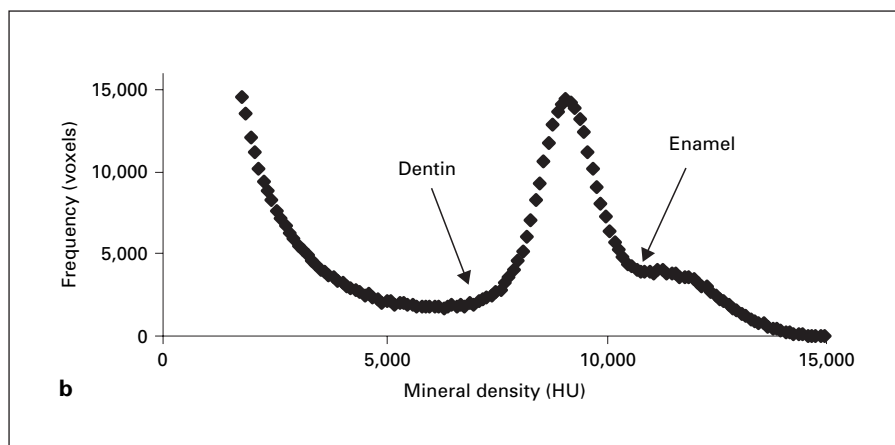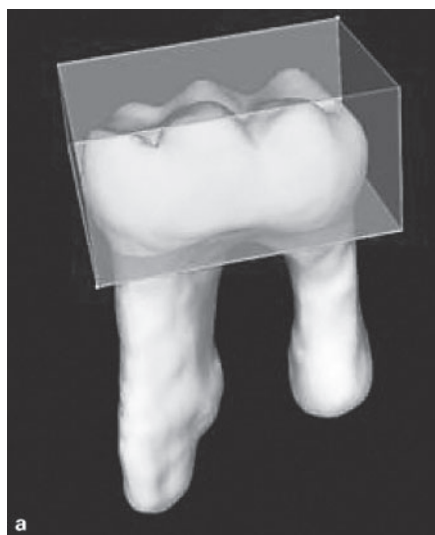
Fig. 2. FTIR microspectroscopic analysis of the trabecular bone of male BGN-KO and age- and sex-matched WT mice. Mean values from multiple (5–12) spectra obtained at sites below the epiphysis are shown. The mineral-to-matrix ratio (**a**) was decreased in KO compared with WT trabeculae at all ages, with statistical significance (* $p < 0.05$) in the youngest and oldest bones. Crystallinity (**b**) was significantly increased in the 3-week bones, but was equivalent to WT mice in the older bones. The carbonate-to-phosphate ratio (**c**) did not vary significantly between KO and WT trabeculae, but did increase with age in all bones.

Fig. 3. Micro-CT analysis of mouse molar crowns. **a** Typical 3-dimensional reconstruction of a BGN-KO and age- and sex-matched WT first molar crown at 3 months. **b** Histogram of 3-dimensional density allows easy separation of enamel and dentin contributions in the BGN-KO and WT teeth. HU = Hounsfield unit. **c** Mean and standard deviation for crown volumes of first and second molars in male and female BGN-KO and WT animals. [a] $p < 0.05$ compared with the same tooth in WT mice; [b] $p < 0.05$ compared with the same tooth, the same genotype in males.
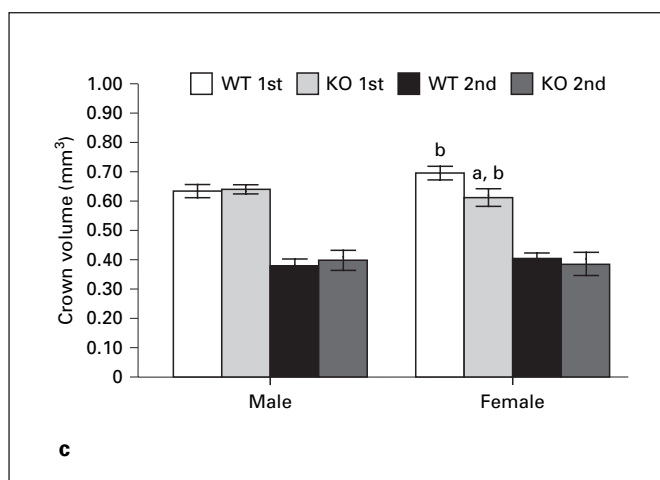
FTIRI of BGN- and DCN-KO Teeth

Typical spatial variation in mineral and matrix properties of first molars of 3-month-old male BGN- (n = 4) and DCN-deficient (n = 3) animals were compared (fig. 4a–d) with those of sex- and background-matched controls (n = 3). The mineral-to-matrix ratio (fig. 4a) visually appeared slightly higher in the BGN-KO teeth, compared with the WT and DCN-KO teeth. Crystallinity, measured as the 1030 cm^{-1}/1020 cm^{-1} intensity ratio (fig. 4b), appeared to have a comparable distribution in all three genotypes. In contrast, the carbonate-to-amide I peak area ratio visually appeared appreciably higher in all BGN-deficient first molars in relation to the other genotypes. The 1660 cm^{-1}/1690 cm^{-1} intensity ratio, indicative of collagen maturity, also appeared higher in the BGN-deficient teeth. Figure 5 compares the average for each of the above-mentioned parameters observed for each image in the 10 teeth analyzed. There was no statistically significant difference in the mineral-to-matrix ratio, although there was a sharper distribution in the BGN-deficient animals as seen in the pixel histograms (data not shown). There was no significant difference in the crystallinity parameter, although it was slightly increased in both BGN- and DCN-deficient molars in relation to WT molars. The carbonate-to-amide I ratio was significantly decreased in the BGN-KO molars and significantly increased in the DCN-KO molars compared with controls, while the 1660 cm^{-1}/1690 cm^{-1} ratio was slightly increased in the BGN-KO molars, but had a broader distribution. The pixel distribution showed a greater population of low and high values in the molars of BGN-KO mice (data not shown).
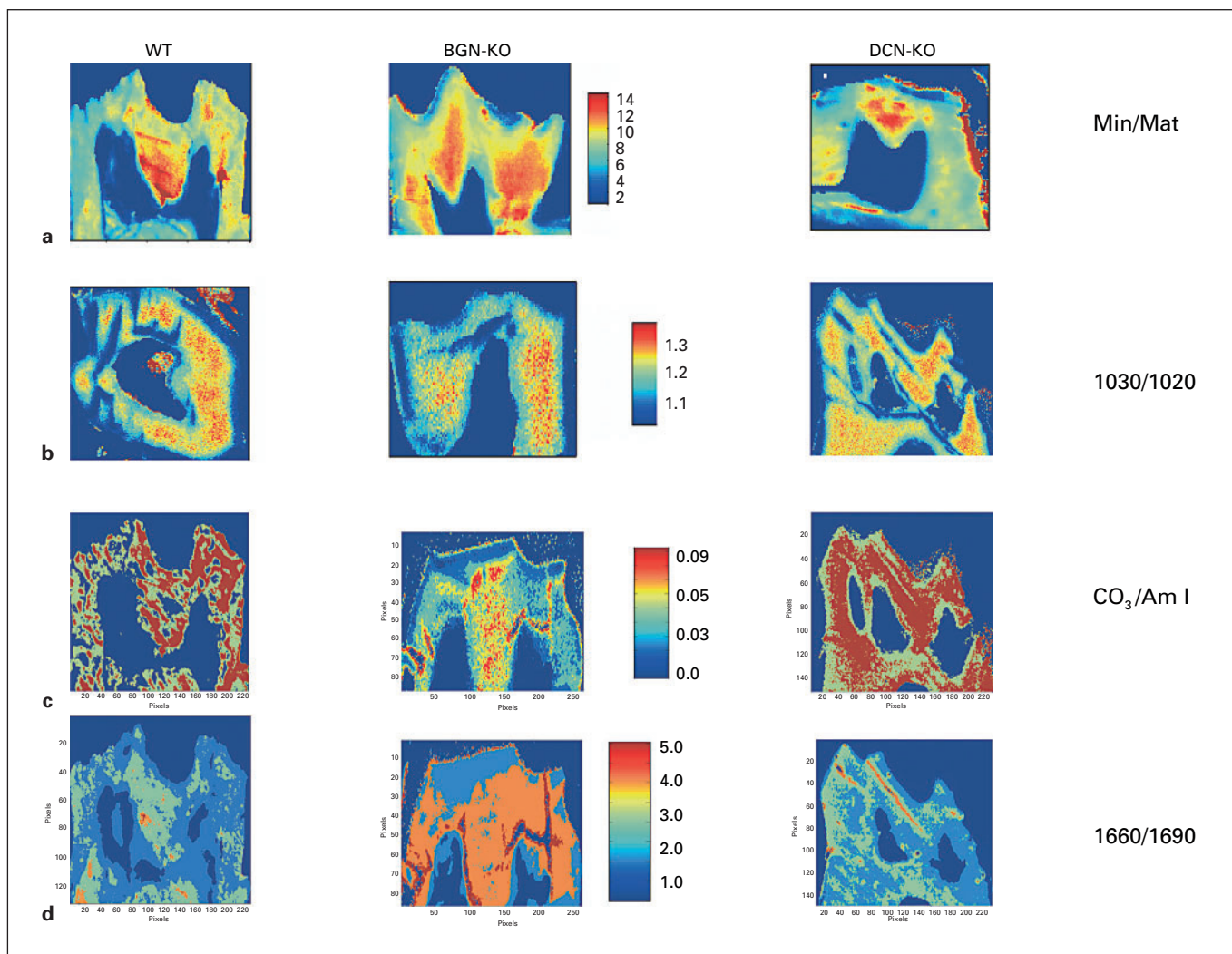
Fig. 4. Infrared imaging of first molars from several different 3-month-old male BGN-KO, DCN-KO, and age- and sex-matched WT teeth. Typical images of mineral-to-matrix (Min/Mat) ratio (**a**), crystallinity (1030 cm^{-1}/ 1020 cm^{-1} intensity ratio) (**b**), carbonate-to-amide I (CO_3/Am I) (**c**), and collagen (1660 cm^{-1}/1690 cm^{-1} intensity ratio) (**d**) maturity. Color scales for each category of images are identical. Each image is approximately 750 × 850 μm^2.

Discussion

This report highlights the use of micro-CT and FTIR microscopy and microscopic imaging to obtain new information, not derivable from light or electron microscopy, about the mineral and matrix composition of bones and teeth. We have extensively used the FTIR technique in the analysis of bones of mutant animals [Boskey and Mendelsohn, 2005], but this report is the first to document the use of infrared imaging to characterize changes in rodent teeth. Differences between bone and tooth

properties in the BGN-KO mouse provide additional insights into the effects of this protein.

BGN-KO Bones and Teeth Show Different Patterns of Mineral Alterations

The BGN-deficient bones at all ages analyzed were thinner, mechanically weaker, and had distinct material properties compared with WT animals [Xu et al., 1998]. The detailed material analysis of the bones based on infrared microspectroscopy showed that the more recently formed bone adjacent to the periosteum and in the center

Fig. 5. Variation in FTIR parameters in 3-month-old male BGN-KO, DCN-KO, and age-, background- (C3H), and sex-matched WT teeth; mean and standard deviations from 3–5 images of each first molar. * $p < 0.05$. Min/Mat = Mineral-to-matrix ratio; 1030/1020 = 1030 cm^{-1}/1020 cm^{-1} intensity ratio; 1660/1690 = 1660 cm^{-1}/1690 cm^{-1} intensity ratio; CO$_3$/Am I = carbonate-to-amide I ratio.
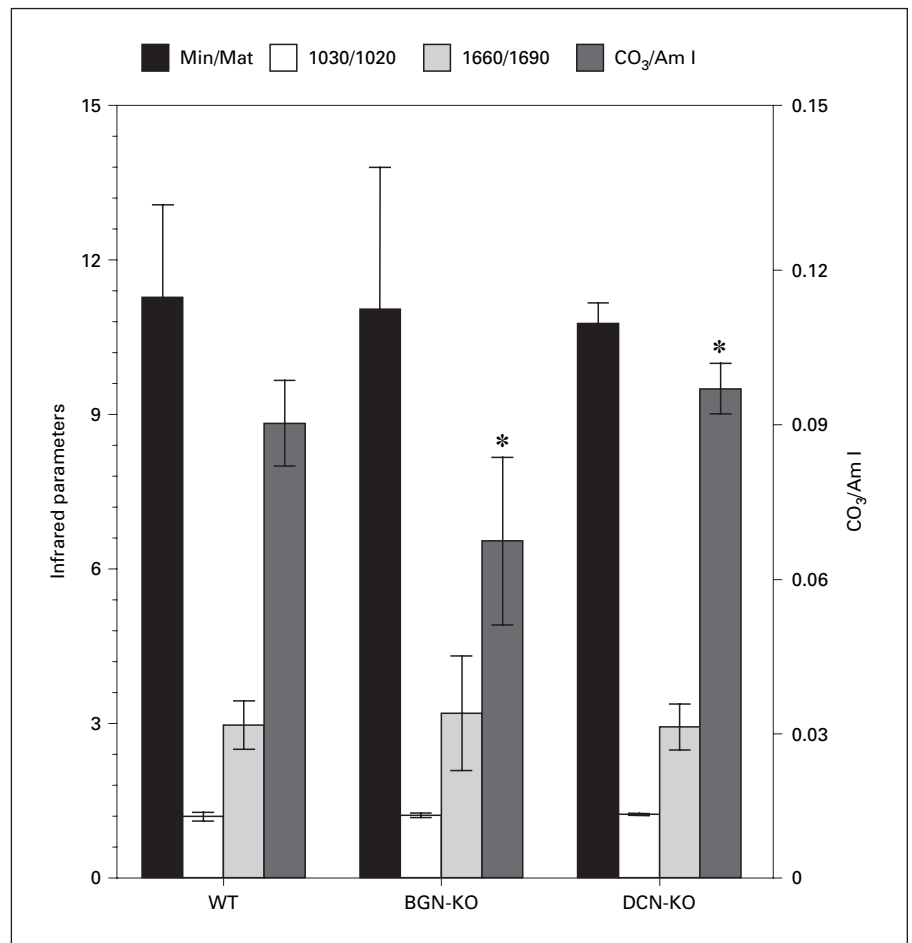
of the cortex showed the most difference from WT controls, suggesting an effect of BGN on mineral formation rather than remodeling, as was seen in the bone adjacent to the endosteal surface in the osteocalcin [Boskey et al., 1998] and osteopontin [Boskey et al., 2002] KO mice. The BGN-KO bone contained a lower mineral-to-matrix ratio, but had larger (more perfect) crystals. Since the collagen fibrils within the BGN-KO bone tend to be larger [Corsi et al., 2002], this could be due to a lack of appropriate sites for new mineral deposition within the collagen itself, since collagen forms the template upon which the mineral is deposited [Gokhale et al., 2001]. Thus, the observed changes in material properties might be an indirect effect of the modification of the collagen fibrils. BGN regulates the collagen fibril diameter, both in vitro and in the tissues of KO animals [Goldberg et al., 2003]. On the other hand, an initial study showed that cartilage BGN and a mixture of SLRPs isolated from bone were HA nucleators [Boskey et al., 1997]. This would suggest that

in the absence of BGN, there would be fewer nucleation sites, although bone has more than one matrix protein involved in nucleation. With fewer nucleation sites, and the same local calcium and phosphate concentrations, those nuclei that are present would tend to grow to a larger size, hence the observed increased crystallinity in the BGN-KO bones. It is important to note that the material properties of the DMP-1 KO bones are similar to those of the BGN-KO bones (lower mineral-to-matrix ratio and larger crystals) [Ling et al., 2005], and DMP-1 is also a HA nucleator [Tartaix et al., 2004].

The phenotype in the BGN-KO tooth was quite different from the bone. There was no significant reduction in mineral content in the teeth; in contrast, there was no difference in mineral content (mineral-to-matrix ratio) in relation to WT controls. Crystal size was not significantly altered, but the relative carbonate content, which in both bone [Tarnowski et al., 2002] and dentin increases with tissue age [Coklica et al., 1969], was decreased in the

BGN-KO teeth. Additionally, while the BGN-KO bone has thicker collagen fibrils, the BGN-deficient tooth has thinner ones [Goldberg et al., 2002]. The presence of thinner collagen fibrils in the dentin might suggest that there would be more sites for initiation of mineralization, although earlier electron microscopic studies of primary mineralization in calvaria reported that DCN disappears and fibrils fuse prior to mineral deposition [Hoshi et al., 1999]. Similar data are not available for BGN. Even in the absence of one of the potential HA nucleators, the number of sites on collagen might be closer to normal in the tooth, thus there would be a lesser difference in mineral content in the tooth, and hence, a lesser change in crystallinity. The decreased carbonate content in the BGN-deficient molar suggests impaired or delayed mineralization, but this is difficult to reconcile in the absence of data from younger animals. The increased carbonate content in the DCN-deficient teeth, in the absence of other changes in material properties, suggests that the mineral is older, but again, additional studies on younger animals are needed.

It should be noted that the BGN-deficient bone and dentin studies were done in mice from different backgrounds; however, based on preliminary analyses of the bones of the C3H BGN-KO mice, we do not think that this is a major contributor to the difference. It is much more likely that the different material properties observed are tissue specific, rather than background specific. Since bones in the DCN-deficient mice like those in the BGN-deficient mice have smaller fibril diameters [Corsi et al., 2002], it will be interesting to characterize the bones in the DCN-deficient mice.

Sex-Dependent Differences in WT and BGN-Deficient Teeth

The BGN gene is located on human [McBride et al., 1990] and mouse [Chatterjee et al., 1993] X chromosomes, and thus, in males, has no second allele (on Y). In females, normally, one allele is inactivated so that men and women have equal amounts of BGN expression. Initial analyses were performed only on the bones of males lacking BGN. Yet the female mice, like female children with Turner syndrome who lack BGN [Heegard et al., 1997] and may fail to express another factor that controls BGN expression, showed greater differences in tooth volume than male mice. In that respect, it is interesting to note that human males with Klinefelter syndrome (XXY), who may express extra BGN, have larger permanent tooth crowns than normal males and females [Alvesalo et al., 1991]. There are no consistent reports of sexual dimorphism in crown size in humans and primates, although several studies have addressed this question [Dempsey et al., 1999; Koppe and Swindler, 2004; Anderson, 2005; Harris and Lease, 2005]. This report is the first to note sexual dimorphism in crown size in mice.

Conclusions

Variations in mineral properties in bones and teeth contribute to the mechanical performance of these tissues. Genetically derived mutant animals lacking one or more extracellular matrix component are being studied to provide insight not only into the mechanical strength and geometry of these tissues, but also, as described in this review, into the functions of the proteins that are ablated. Combing these data with histology, gene expression data, mechanical testing, and cell culture studies will certainly facilitate the understanding of more than one of the functions of these proteins.

Acknowledgments

References

Akesson, K., M.D. Grynpas, R.G. Hancock, R. Odselius, K.J. Obrant (1994) Energy-dispersive X-ray microanalysis of the bone mineral content in human trabecular bone: a comparison with ICPES and neutron activation analysis. Calcif Tissue Int 55: 236–239.

Alvesalo, L., E. Tammisalo, G. Townsend (1991) Upper central incisor and canine tooth crown size in 47,XXY males. J Dent Res 70: 1057–1060.

Ameye, L., M.F. Young (2002) Mice deficient in small leucine-rich proteoglycans: novel in vivo models for osteoporosis, osteoarthritis, Ehlers-Danlos syndrome, muscular dystrophy, and corneal diseases. Glycobiology 12: 107R–116R.

Anderson, A.A. (2005) Dentition and occlusion development in African American children: mesiodistal crown diameters and tooth-size ratios of primary teeth. Pediatr Dent 27: 121–128.

Bonar, L.C., M. Shimizu, J.E. Roberts, R.G. Griffin, M.J. Glimcher (1991) Structural and composition studies on the mineral of newly formed dental enamel: a chemical, X-ray diffraction, and 31P and proton nuclear magnetic resonance study. J Bone Miner Res 6: 1167–1176.

Boskey, A.L. (2001) Bone mineralization; in Cowin, S.C. (ed): Bone Biomechanics, ed 3. Boca Raton, CRC Press, pp 5.1–5.34.

Boskey, A.L. (2003) Bone mineral crystal size. Osteoporos Int *14(suppl 5):* 16–21.

Boskey, A.L., S. Gadaleta, C. Gundberg, S.B. Doty, P. Ducy, G. Karsenty (1998) Fourier transform infrared microspectroscopic analysis of bones of osteocalcin-deficient mice provides insight into the function of osteocalcin. Bone *23:* 187–96.

Boskey, A.L., R. Mendelsohn (2005) Infrared spectroscopic characterization of mineralized tissues. Vibrational Spectroscopy *38:* 107–114.

Boskey, A.L., L. Spevak, S.B. Doty, L. Rosenberg (1997) Effects of bone CS-proteoglycans, DS-decorin, and DS-biglycan on hydroxyapatite formation in a gelatin gel. Calcif Tissue Int *61:* 298–305.

Boskey, A.L., L. Spevak, E. Paschalis, S.B. Doty, M.D. McKee (2002) Osteopontin deficiency increases mineral content and mineral crystallinity in mouse bone. Calcif Tissue Int *71:* 145–154.

Chatterjee, A., C.J. Faust, G.E. Herman (1993) Genetic and physical mapping of the biglycan gene on the mouse X chromosome. Mamm Genome *4:* 33–36.

Chen, X.D., S. Shi, T. Xu, P.G. Robey, M.F. Young (2002) Age-related osteoporosis in biglycan-deficient mice is related to defects in bone marrow stromal cells. J Bone Miner Res *17:* 331–340.

Coklica, V., F. Brudevold, B.H. Amdur (1969) The distribution and composition of density fractions from human crown dentine. Arch Oral Biol *14:* 451–460.

Corsi, A., T. Xu, X.D. Chen, A. Boyde, J. Liang, M. Mankani, B. Sommer, R.V. Iozzo, I. Eichstetter, P.G. Robey, P. Bianco, M.F. Young (2002) Phenotypic effects of biglycan deficiency are linked to collagen fibril abnormalities, are synergized by decorin deficiency, and mimic Ehlers-Danlos-like changes in bone and other connective tissues. J Bone Miner Res *17:* 1180–1189.

Danielson, K., H. Baribault, D. Holmes, H. Graham, K. Kadler, R. Iozzo (1997) Targeted disruption of decorin leads to abnormal collagen fibril morphology and skin fragility. J Cell Biol *136:* 729–749.

Dempsey, P.J., G.C. Townsend, L.C. Richards (1999) Increased tooth crown size in females with twin brothers: evidence for hormonal diffusion between human twins in utero. Am J Hum Biol *11:* 577–586.

Ducy, P., C. Desbois, B. Boyce, G. Pinero, B. Story, C. Dunstan, E. Smith, J. Bonadio, S. Goldstein, C. Gundberg, A. Bradley, G. Karsenty (1996) Increased bone formation in osteocalcin-deficient mice. Nature *382:* 448–452.

Feng, J.Q., H. Huang, Y. Lu, L. Ye, Y. Xie, T.W. Tsutsui, T. Kunieda, T. Castranio, G. Scott, L.B. Bonewald, Y. Mishina (2003) The dentin matrix protein 1 (Dmp1) is specifically expressed in mineralized, but not soft, tissues during development. J Dent Res *82:* 776–780.

Genant, H.K., C. Gordon, Y. Jiang, T.M. Link, D. Hans, S. Majumdar, T.F. Lang (2000) Advanced imaging of the macrostructure and microstructure of bone. Horm Res *54(suppl 1):* 24–30.

Gokhale, J., P.G. Robey, A.L. Boskey (2001) The biochemistry of bone; in Marcus, R., D. Feldman, J. Kelsey (eds): Osteoporosis, ed 2. San Diego, Academic Press, vol 1, pp 107–189.

Goldberg, M. (2002) Biglycan is a repressor of amelogenin expression and enamel formation: an emerging hypothesis. J Dent Res *81:* 520–524.

Goldberg, M., O. Rapoport, D. Septier, K. Palmier, R. Hall, G. Embery, M. Young, L. Ameye (2003) Proteoglycans in predentin: the last 15 micrometers before mineralization. Connect Tissue Res *44(suppl 1):* 184–188.

Harris, E.F., L.R. Lease (2005) Mesiodistal tooth crown dimensions of the primary dentition: a worldwide survey. Am J Phys Anthropol *128:* 593–607.

Heegaard, A.M., P. Gehron Robey, W. Vogel, W. Just, R.L. Widom, J. Scholler, L.W. Fisher, M.F. Young (1997) Functional characterization of the human biglycan 5′-flanking DNA and binding of the transcription factor c-Krox. J Bone Miner Res *12:* 2050–2060.

Hocking, A.M., T. Shinomura, D.J. McQuillan (1998) Leucine-rich repeat glycoproteins of the extracellular matrix. Matrix Biol *17:* 1–19.

Hoshi, K., S. Kemmotsu, Y. Takeuchi, N. Amizuka, H. Ozawa (1999) The primary calcification in bones follows removal of decorin and fusion of collagen fibrils. J Bone Miner Res *14:* 273–280.

Iozzo, R.V. (1998) Matrix proteoglycans: from molecular design to cellular function. Annu Rev Biochem *67:* 609–652.

Kirkham, J., S.J. Brookes, R.C. Shore, W.A. Bonass, D.A. Smith, M.L. Wallwork, C. Robinson (1998) Atomic force microscopy studies of crystal surface topology during enamel development. Connect Tissue Res *38:* 91–100.

Koppe, T., D.R. Swindler (2004) Metric sexual dimorphism in the deciduous teeth of Old World monkeys. Ann Anat *186:* 367–374.

Landis, W.J., M. Navarro, J.R. Neuringer, K. Kurz (1984) Single bovine enamel particles examined by electron optics. J Dent Res *63:* 629–634.

Ling, Y., H.F. Rios, E.R. Myers, Y. Lu, J.Q. Feng, A.L. Boskey (2005) DMP1 depletion decreases bone mineralization in vivo: an FTIR imaging analysis. J Bone Miner Res *20:* 2169–2177.

McBride, O.W., L.W. Fisher, M.F. Young (1990) Localization of PGI (biglycan, BGN) and PGII (decorin, DCN, PG-40) genes on human chromosomes Xq13-qter and 12q, respectively. Genomics *6:* 219–225.

Otsu, N. (1979) A threshold selection method from gray-level histograms. IEEE Trans Syst Man Cybern *9:* 62–66.

Peru, L., G. Daculsi (1994) Synthetic calcium phosphates: models for biological crystals? Clin Mater *15:* 267–272.

Posner, A.S., R.A. Beebe (1975) The surface chemistry of bone mineral and related calcium phosphates. Semin Arthritis Rheum *4:* 267–291.

Robey, P.G. (1996) Vertebrate mineralized matrix proteins: structure and function. Connect Tissue Res *35:* 131–136.

Roschger, P., H. Plenk, Jr., K. Klaushofer, J. Eschberger (1995) A new scanning electron microscopy approach to the quantification of bone mineral distribution: backscattered electron image grey-levels correlated to calcium K alpha-line intensities. Scanning Microsc *9:* 75–86.

Tarnowski, C.P., M.A. Ignelzi, Jr., M.D. Morris (2002) Mineralization of developing mouse calvaria as revealed by Raman microspectroscopy. J Bone Miner Res *17:* 1118–1126.

Tartaix, P.H., M. Doulaverakis, A. George, L.W. Fisher, W.T. Butler, C. Qin, E. Salih, M. Tan, Y. Fujimoto, L. Spevak, A.L. Boskey (2004) In vitro effects of dentin matrix protein-1 on hydroxyapatite formation provide insights into in vivo functions. J Biol Chem *279:* 18115–18120.

Tommasini, S.M., T.G. Morgan, M.C.H. van der Meulen, K.J. Jepsen (2005) Genetic variation in structure-function relationships for the inbred mouse lumbar vertebral body. J Bone Miner Res *20:* 817–827.

Tong, W., M.J. Glimcher, J.L. Katz, L. Kuhn, S.J. Eppell (2003) Size and shape of mineralites in young bovine bone measured by atomic force microscopy. Calcif Tissue Int *72:* 592–598.

Xu, T., P. Bianco, L.W. Fisher, G. Longenecker, E. Smith, S. Goldstein, J. Bonadio, A. Boskey, A.M. Heegaard, B. Sommer, K. Satomura, P. Dominguez, C. Zhao, A.B. Kulkarni, P.G. Robey, M.F. Young (1998) Targeted disruption of the biglycan gene leads to an osteoporosis-like phenotype in mice. Nat Genet *20:* 78–82.